Supporting Information for:

Slow Magnetic Relaxation Induced by a Large Transverse Zero-Field Splitting in a $Mn^{II}Re^{IV}(CN)_2$ Single-Chain Magnet

Xiaowen Feng[1], Junjie Liu[2], T. David Harris[1], Stephen Hill*[3] and Jeffrey R. Long*[1]

[1]*Department of Chemistry, University of California, Berkeley, California 94720, USA,*
[2]*Department of Physics, University of Florida. Gainesville, Florida, 32611, USA*
[3] *Department of Physics and National High Magnetic Field Laboratory, Florida State University, Tallahassee, Florida, 32310, USA*

J. Am. Chem. Soc.

Table of Contents

Table S1. Crystallographic data[a] for $(DMF)_4ZnReCl_4(CN)_2$ and $[(PY5Me_2)Mn]_2[ReCl_4(CN)_2](PF_6)_2$

	2	**3**
formula	$C_{14}H_{28}Cl_4ZnN_6O_4Re$	$C_{56}H_{50}N_{12}P_2F_{12}Cl_4MnRe$
fw	737.81	1064.91
T, K	100	100
space group	*P* 1	*P*2(1)/c
Z	1	2
a, Å	8.6226(8)	13.7430(2)
b, Å	10.3074(10)	21.9421(2)
c, Å	10.4929(10)	12.8569(1)
α, deg	104.878(4)	90.000
β, deg	92.699(4)	107.514(3)
γ, deg	101.666(4)	90.000
V, Å^3	877.85(14)	3697.28 (10)
d_{calc}, g/cm^3	1.592	1.451
R_1 (wR_2), %[b]	2.15 (5.70)	5.45 (14.20)

[a]Obtained with graphite-monochromated Cu Kα (λ = 1.5406 Å) for **2** and **3**. [b] $R_1 = \Sigma||F_o| - |F_c||/\Sigma|F_o|$, $wR_2 = \{\Sigma\ [w(F_o^2 - F_c^2)^2]\}^{1/2}$.

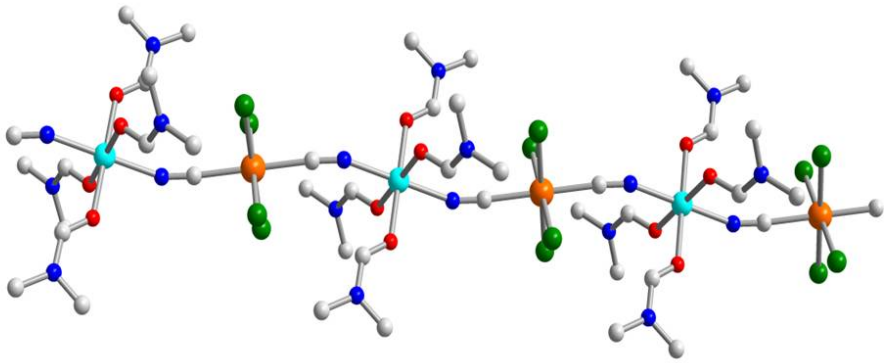

Figure S1. Crystal structure of $(DMF)_4ZnReCl_4(CN)_2$ **2** chain. Orange, cyan, green, red, blue, and gray spheres represent rhenium, zinc, chlorine, oxygen, nitrogen, and carbon atoms, respectively; hydrogen atoms have been omitted for clarity.

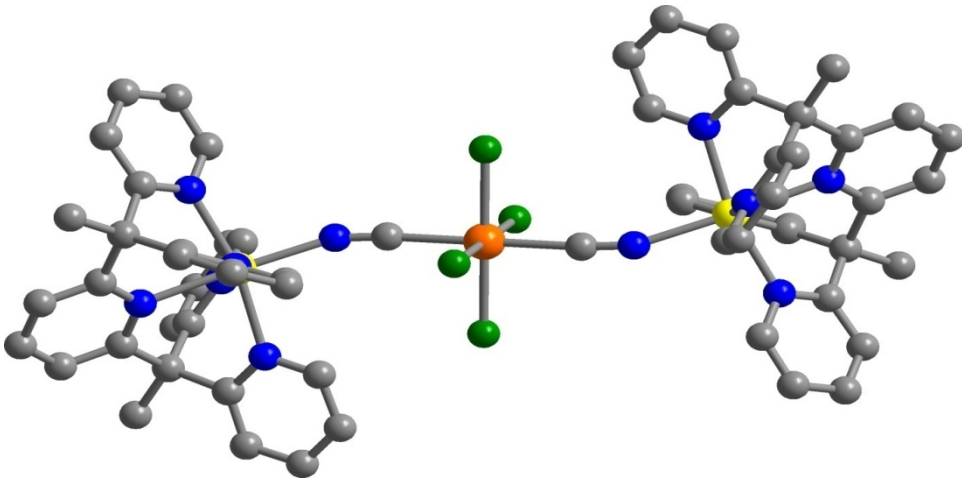

Figure S2. Crystal structure of $\{[(PY5Me_2)Mn]_2[ReCl_4(CN)_2]\}^{2+}$ (**3**). Orange, yellow, green, blue, and gray spheres represent rhenium, manganese, chlorine, nitrogen, and carbon atoms, respectively; hydrogen atoms have been omitted for clarity.

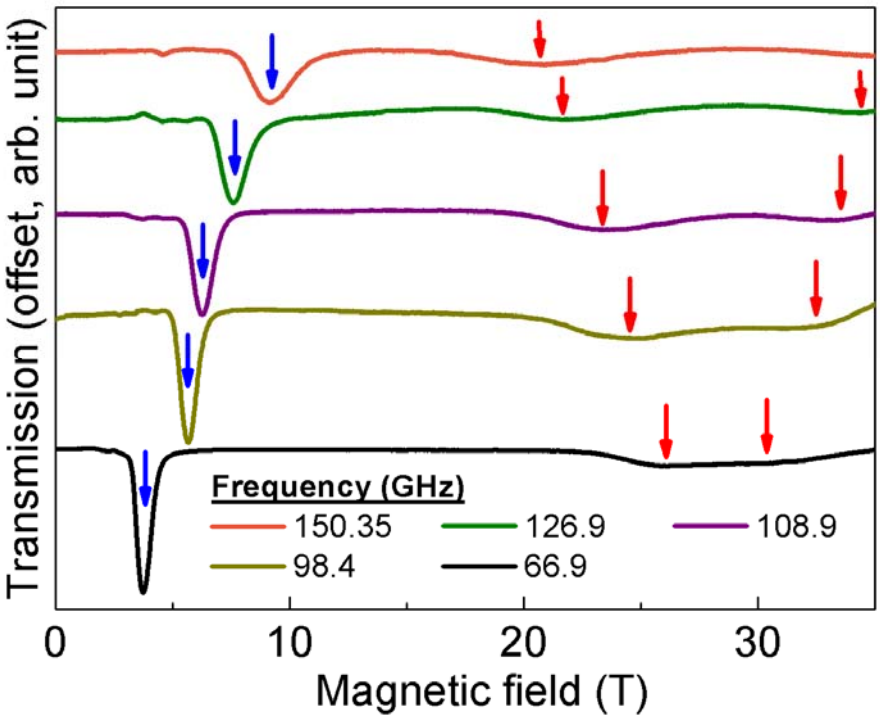

Figure S3. Single-crystal high-field EPR spectra collected at various frequencies in the range from 66.9 to 150 GHz and at T = 1.4 K, with the field applied 3° away from the molecular *z*-axis. The spectra are normalized according to the weight (area) associated with the low-field intra-Kramers resonance (indicated by the blue arrows). The observation of three resonances between 66 GHz and 127 GHz (one intra-Kramers and two broad inter-Kramers transitions denoted by red arrows) provides unambiguous evidence for the easy-plane anisotropy; a more detailed discussion is given in the main text and in the caption to Figure S4.

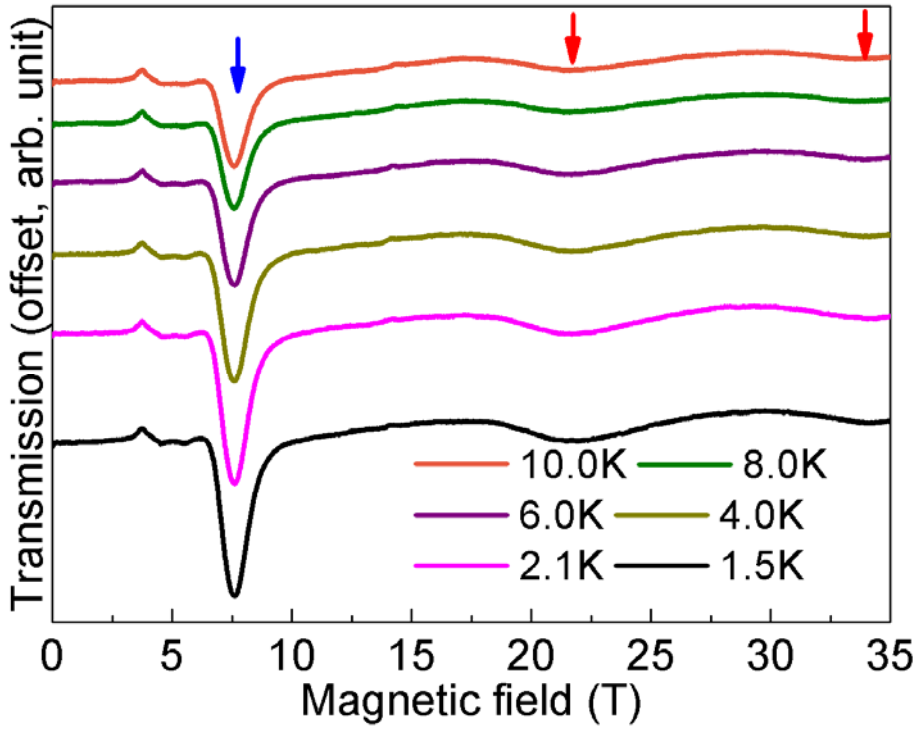

Figure S4. Temperature dependence spectra collected at f = 126.9 GHz. All three resonances strengthen and persist to the lowest temperature, where $k_BT << hf$. This indicates that of all the transitions correspond to excitations from the ground state of the molecule, with the blue and red arrows denoting intra- and inter-Kramers transitions, respectively.

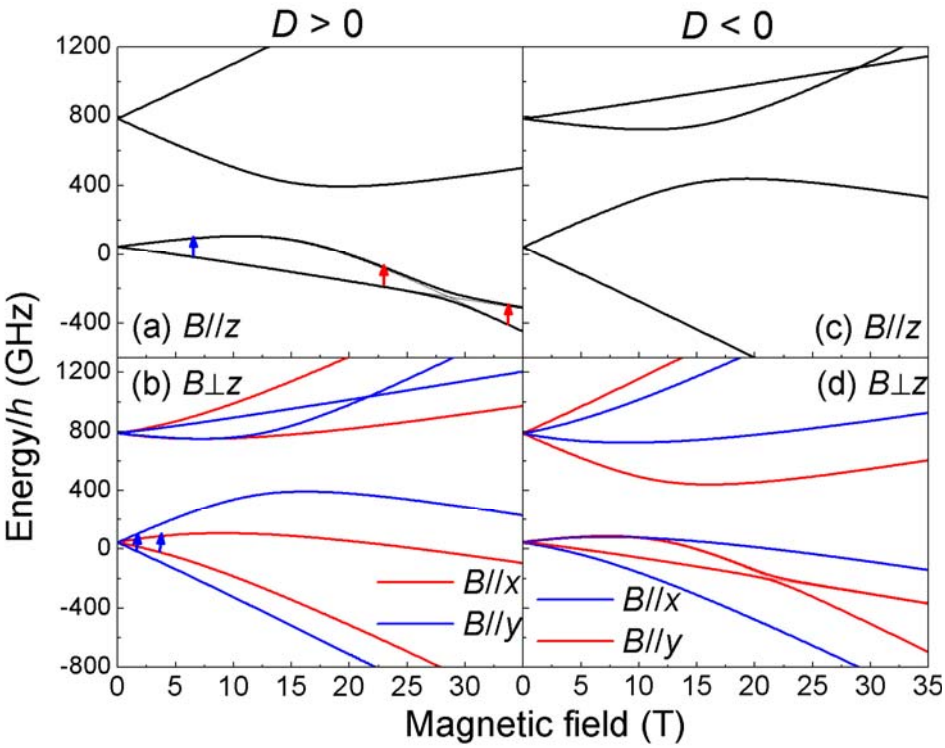

Figure S5. Simulations of the Zeeman diagrams based on the Hamiltonian of Eqn. (1), with $B//z$ [(a) and (c)] and $B\perp z$ [(b) and (d)], for the two cases $D > 0$ [(a) and (b)] and $D < 0$ [(c) and (d)]. The employed magnitudes of the employed parameters are those determined for complex **1** given in the main text. Panel (a) corresponds exactly to the black curves in Fig. 3; the thick black curve includes a 3° misalignment of the applied field, corresponding to the actual experimental situation. The red and blue arrows in (a) correspond to allowed EPR transitions of ~100 GHz, illustrating the intra-Kramers transition (red) and the two inter-Kramers (blue) transitions observed in the single-crystal EPR studies. Panel (b) displays the Zeeman diagrams with $B//x$ and $B//y$; the blue arrows denote the ~100 GHz intra-Kramers x & y components of the powder spectra seen in Figs. 2 and S4. As can be seen, panels (a) and (b) reproduce all aspects of the single-crystal and powder EPR experiments remarkably well. Panels (c) and (d) depict the corresponding Zeeman diagrams generated with $D < 0$. As seen in (d), it is possible to produce a spectrum consisting of three ground state resonances for the $D < 0$, $B//x$ case. However, in order to obtain quantitative agreement with the single-crystal and powder EPR data, unphysical E ($> |D|/3$) and/or g (> 2) parameters are obtained. This rules out the $D < 0$ parameterization – see main article for a more detailed discussion.

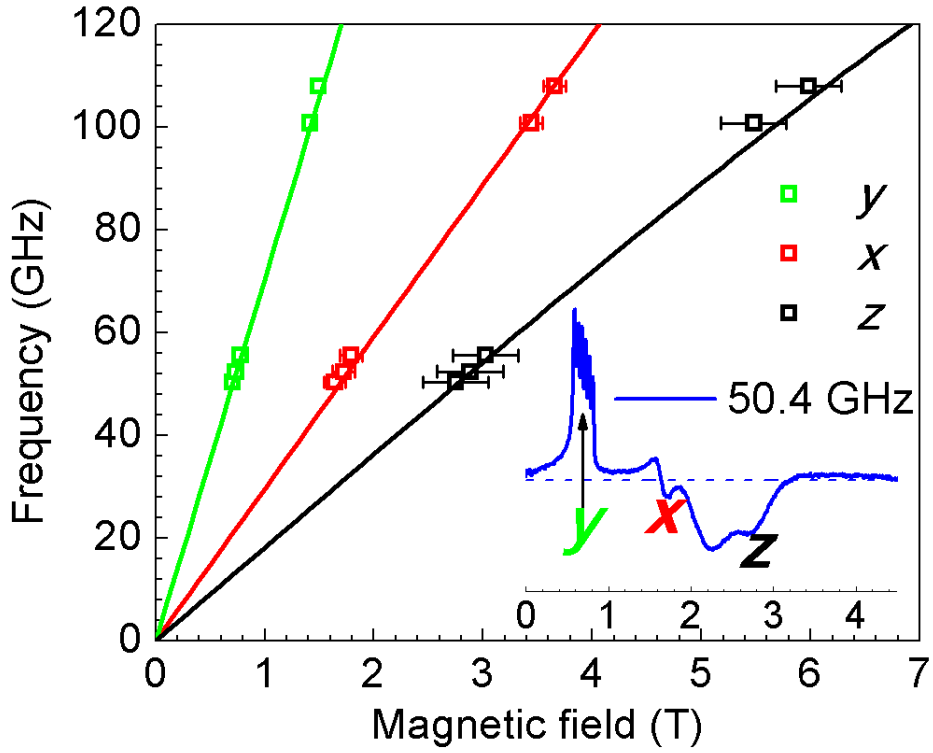

Figure S6. Frequency dependence of the high-frequency EPR peak positions deduced from studies of a powder sample of **1** at 5 K; a representative spectrum collected in the first-derivative mode at 50.4 GHz is displayed in the inset. Three branches of the resonances are observed, corresponding to the three principal components of the effective Lande g tensor associated with lowest Kramers doublet (field parallel to *x*, *y* and *z*). The fine structure seen in the *y*-component is due to nuclear hyperfine splitting; the resonance position is chosen at the center of the fine structure spectrum. The solid lines in the main panel are simulations of the three resonance branches employing Eqn. (1) and the unique set of parameters given in the main article. The fine structure seen in the **y**-component is due to nuclear hyperfine splitting; the resonance position is chosen at the center of the fine structure spectrum. We note that the hyperfine splitting is not observed in the x or z components, or in the y component at higher frequencies, suggesting that it is washed out at higher fields due to g-strain.

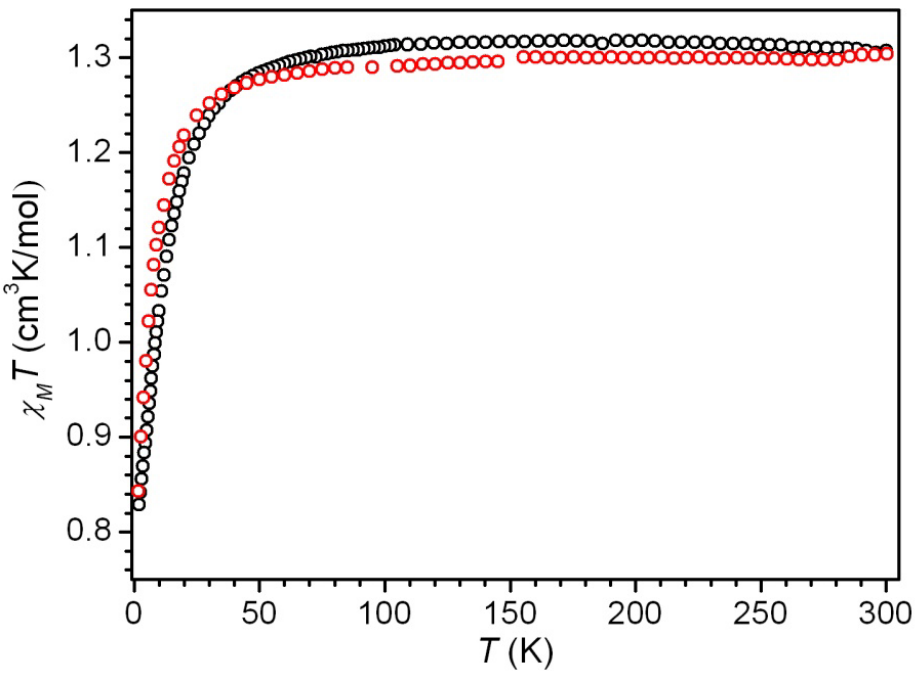

Figure S7. Variable-temperature dc magnetic susceptibility data for $(Bu_4N)_2[ReCl_4(CN)_2]\cdot 2DMA$ (**1**, black) and $(DMF)_4ZnReCl_4(CN)_2$ (**2**, red), collected in an applied field of 1000 Oe. The nearly superimposable data sets indicate that the Re^{IV} ions well-isolated magnetically in both **1** and **2**.

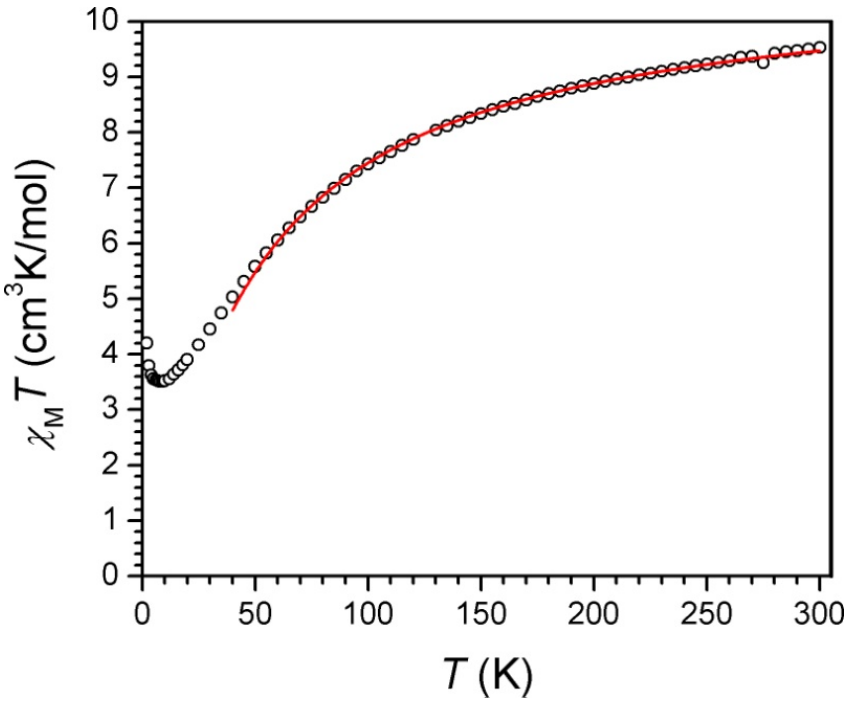

Figure S8. Variable-temperature dc magnetic susceptibility data for $[(PY5Me_2)_2Mn]_2ReCl_4(CN)_2](PF_6)_2$ (**3**), collected in an applied field of 1000 Oe. The solid red line corresponds to a fit to the data, with $J = -3.0$ cm^{-1} and $g = 1.98$